Interconnected vector pairs image conditions: new possibilities for visualization of acoustical media

Gennady Erokhin, Leonid Pestov, Aleksandr Danilin and Maksim Kozlov, Immanuel Kant Baltic Federal University; Dmitrii Ponomarenko, Octopus Ltd.*

Summary

Reflection or scattering of acoustical wave on an obstacle at any moment may be considered as interaction of two interconnected vectors: the particle velocity vector of the incident wave and the generated vector of the reflected or scattered wave. In this paper an accurate statistical analysis of the amplitudes and phases of the interconnected vectors for the whole ensemble of the time samples and sources is proposed. We have developed interconnected vector pairs image conditions that give a new look on visualization of acoustical media.

Introduction

Every point of inhomogeneous acoustic medium (when a wave propagates through) is a source of secondary radiation that may be registered at the day surface. The mathematical methods designed in geophysics can gather the wave field at the day surface and migrate it back into the media. It is mostly developed in the wave-equation-based methods, particularly in the reverse time migration method (RTM) (Baysal et.al.,1983; Whitmore, 1983; McMechan, 1983), where mathematical formalism of the adjoint problem is used (so-called the adjoint state method, Plessix, 2006). This method is an important part of full waveform inversion (Alekseev and Erokhin, 1989; Symes, 2007; Xie, 2015; Alkhalifah, 2015) and describes the gradient of the objective function under optimization with respect to velocity. The calculation of this gradient is an ill-posed problem and requires regularization (Anikonov et.al, 1997). For RTM such regularization is performed by filtration in an extended space of parameters, so-called extending image conditions (Yoon and Marfurd, 2006; Sava and Fomel, 2006; Costa et.al.,2009, Zhang and McMechan, 2011, Vyas et.al., 2011, Yan et.al., 2014).

In this paper we propose a new visualization method of acoustical media based on accurate statistical analysis of the amplitudes and phases of the interconnected vectors. We call it vector pairs reverse time migration (VPRTM) method.

Method

We derive acoustical wave by the couple $(p,\vec{u})$ where p is the pressure and $\vec{u}$ is the particle velocity vector field. They satisfy the first order linear differential equations (Pierce, 1989). The forward wave $(p^f,\vec{u}^f)(x,t;x_s), t\in[0,T]$ satisfies the Cauchy problem

$$\begin{aligned} &p^f{}_t - c^2 div(\nabla \vec{u}^f) = r(t)\delta(x-x_s) \\ &\vec{u}^f_t = \nabla p^f \\ &p^f\big|_{t=0} = 0, \quad \vec{u}^f\big|_{t=0} = 0. \end{aligned} \tag{1}$$

Here $r(t)\delta(x-x_s)$ is the source located at the boundary point $x_s \in \Gamma = \left\{x\in\mathbb{R}^n \middle| x^n = 0,\ n=2,3\right\}$ (δ is the Dirac function, and r is some wavelet), T is the time of observation. Let $p_0 = p^f\big|_{\Gamma\times[0,T]}$ be the "measured" pressure. Then the adjoint problem to the problem (1) is written as follows

$$\begin{aligned} &p^b{}_t - c^2 div(\nabla \vec{u}^b) = 0 \\ &\vec{u}^b_t = \nabla p^b + p_0\delta(x^n)\vec{v}_\Gamma \\ &p^b\big|_{t=\mathrm{T}} = 0, \quad \vec{u}^b\big|_{t=\mathrm{T}} = 0, \end{aligned} \tag{2}$$

where $v_\Gamma = (0,...0,1)$) is the unit normal vector to Γ. We call $(p^b,\vec{u}^b)$ the back wave since it propagates in reversal time. So, forward and back waves include two vector fields: $\vec{u}^f(x,t;x_s)$ and $\vec{u}^b(x,t;x_s)$. In what follows we use these vector fields only. Notice that for every fixed source x_s vector field $\vec{u}^b(\cdot;x_s)$ is generated by $\vec{u}^f(\cdot;x_s)$. Further we will use short notations $f=\vec{u}^f$, $b=\vec{u}^b$.

The typical behavior of the interconnected vector pair (IVP) (f,b) at some fixed x,x_s is presented on Fig. 1.

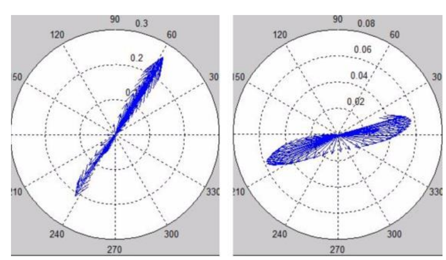

a b

Figure 1: An example of the time-depending pair (f,b) at some fixed point x and fixed x_s. The forward particle velocity vector field f (a) and the back velocity vector field of scattering wave b (b).

Using the statistics of the interconnected vector pairs (f,b) for some set of time samples (around the arrival time $\tau(x,x_s)$) we see that approximately the maximal magnitudes of f are observed for the incident angles $\alpha \simeq 55^\circ$ and 235°. The maximal magnitudes of b are observed for the scattering angles $\beta \simeq 15^\circ$ and 295°. Then one can find the opening angle $\gamma = (\alpha - \beta)/2 \simeq 20^\circ$ and the dip angle $\theta = (\alpha + \beta)/2 \simeq 35^\circ$. Notice that the maximal magnitudes of the scattering wave is almost one order less than the incident one. This example shows that IVP can be used to determine some characteristics of the acoustical media. It may be done at every point x on the basis of IVP statistical analysis on some set of sources and time samples. We introduce interconnected vector pairs image conditions (IVPIC) :

$$I(x) = R_Q(f,b)(x). \tag{3}$$

Here the vector pairs (f,b) are defined on some admissible set Q

$$Q \subseteq \{t_k, x_s | t_k = \tau(x,x_s) + k\Delta t, \quad k = 0,...,N \subset_t, s = 1,...,N_s\}$$

and R_Q is some operator being applied to the pair of vectors (f,b) on Q. We call such pairs of vectors admissible vector pairs. Operator R_Q may be taken as follows:

$$R_Q(f,b)(x) = \sum_{s=1}^{N_s}\sum_{k=0}^{N_k} < f,b > (x;t_k,x_s), \tag{3a}$$

where $<,>$ means scalar product,

$$R_Q(f,b)(x) = \sum_{s=1}^{N_s}\sum_{k=0}^{N_k}(|f||b|)(x;t_k,x_s) \tag{3b}$$

$$R_Q(f,b)(x) = \sum_{s=1}^{N_s}\sum_{k=0}^{N_k}(|b|/|f|)(x;t_k,x_s) \tag{3c}$$

$$R_Q(f,b)(x) = M(|f||b|)/M|f|^2 \tag{3d}$$

where M is the mathematical expectation,

$$R_Q(f,b)(x) = \min_{-\pi \le \theta_0 \le \pi} D(\theta - \theta_0) \tag{3e}$$

where D is variance for admissible set Q,

$$R_Q(f,b)(x) = \arg\min_{\theta_0} D(\theta - \theta_0) \quad , -\pi \le \theta_0 \le \pi \tag{3f}$$

etc.

Notice, that the case $R_Q(f,b) = |f||b|$ is similar to RTM, and the case $R_Q(f,b) =< f,b >$ is similar to inverse scattering image condition (Stolk et.al., 2009, Whitmore and Crawley, 2012). The admissible set Q (filtration) plays an important role. Pairs $(f,b)(x;t_k,x_s)$ such that $(t_k,x_s) \notin Q$ are not taken into account. The design of admissible set Q in angle-domain (α,β) or (θ,γ) similar the filtration on the basis of local image matrix (Xie and Wu, 2002; Yan and Xie, 2009).

Synthetic Data Examples

We consider two-dimensional case. To solve Cauchy problems (1)-(2), we use the finite-difference time domain method with staggered grids in space and time. The spatial derivatives are approximated with 12th accuracy order and time derivatives have second accuracy order. The modeling parameters are the following: the whole computational domain is $17 \times 3.5km$, the spacing step is $5m$ the number of sources is 200, the source step is $50m$ the computational domain for one source is $7 \times 3.5km$, the number of receivers is 701, the receiver interval is $10m$, the time step is $0.4ms$, $r(t)$ is Ricker's wavelet with dominant frequency $40Hz$.

The important problem for RTM-like methods is detecting diffractions on the background of the strong reflections (Landa et al., 1987; Khaidukov et.al., 2004, Zhu and Wu, 2008; Kremlev et.al., 2011; Erokhin et.al., 2012). This problem can successfully be solved on the basis of the proposed IC (3) using a target filtration of vector b subject to amplitude and phase features of distributions for reflection and difraction points. Consider a typical case (see Fig. 2). For any point $(t,s) \in Q$ angles α and β are calculated. These angles determine a point in the square $-180^0 \le \alpha, \beta \le 180^0$. On the Figure 2 the color corresponds to the magnitude of vector $b(t,s)$. We call this representation anlge distribution of magnitudes of vector b at the point x. One can see that angle distribution strongly depends on whether the point x is a point of reflection or a diffraction point. This difference makes it possible to choose R_Q that corresponds to reflection or diffraction points. At that the filtration is performed on the basis of anlge distribution of magnitudes of vector b. The results of such filtrations (relection and diffraction filter) for model of three thin layers (Figure 3) are presented on the Fig. 4.

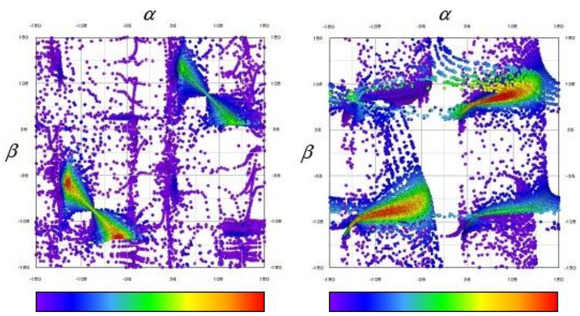

Figure 2: (α,β) -angle distribution of $|\vec{b}|$ at the reflection point (a) and at the diffraction point (b).

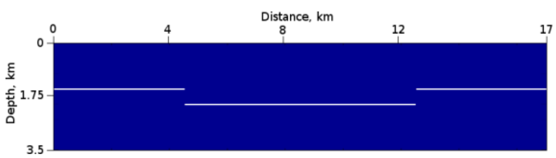

Figure **3**: Model of three thin layers. The velocity is $3km/s$ in the media and $4km/s$ in the layers.

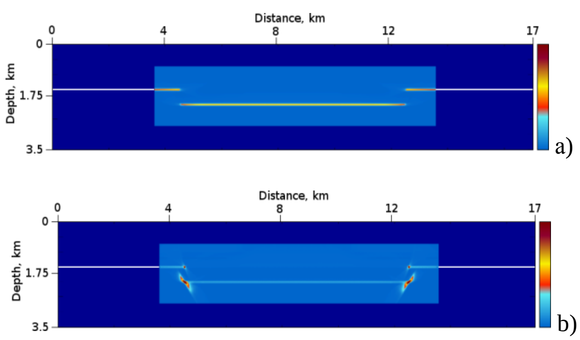

Figure 4: VPRTM. “Reflection” filtration IVPIC (3b) (a) and “diffraction” filtration IVPIC (3b) (b).

The model of two diffractors in homogeneous medium is presented on Fig. 5. Each diffractor is made by velocity jump in one node only. The left diffractor (white) has reduced velocity by $0.1km/s$ w.r.t. background velocity $3km/s$, the right one (red) has increased velocity by $0.1km/s$.

The results of amplitude filtration with different admissible sets are presented on the Fig. 6. The first filter is adapted to extract a negative velocity jump at the diffraction point and the second one is for a positive jump. We call them “soft” and “hard” diffractor filters accordingly. One can see that they form different images for a negative jump (left images) and for a positive jump (right images on the Fig. 6a, 6b). The result of joint filtration (soft and hard) is presented on Fig. 6c. This filtration detects an arbitrary velocity jump.

The result of phase filtration with IVPIC (3f) is presented on the Fig. 6d. In this case the image is much more complicated, and one can see the specific phase images around the diffractor points. These images are different for “soft” and “hard” diffractors. Note that phase filters are more stable than amplitude ones with depth.

The image with IVPIC (3f) for a part of the model Marmousi2 is presented on Fig. 7. We see high phase filter sensitivity w.r.t. small velocity variations. It is confirmed by high correlation between the true velocity and IVPIC (3f).

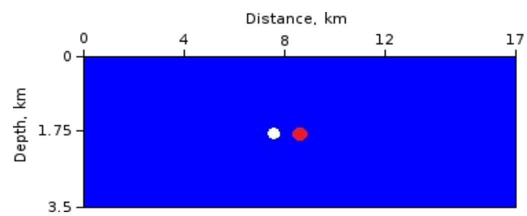

Figure 5: Model of “soft” and “hard” diffractors.

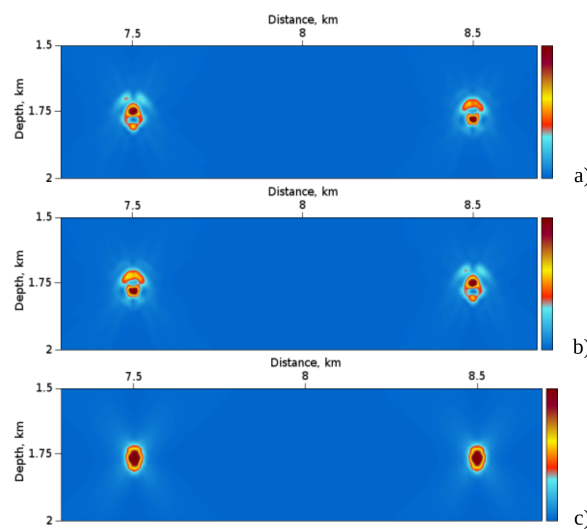

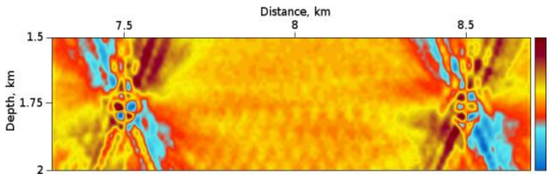

Figure 6**:** VPRTM, "soft" diffractor filter IVPIC (3b) **(**a), "hard" diffractor filter IVPIC (3b) **(**b), "soft+hard" diffractor filter IVPIC (3b**)** (c), phase filter IVPIC (3f) (d).

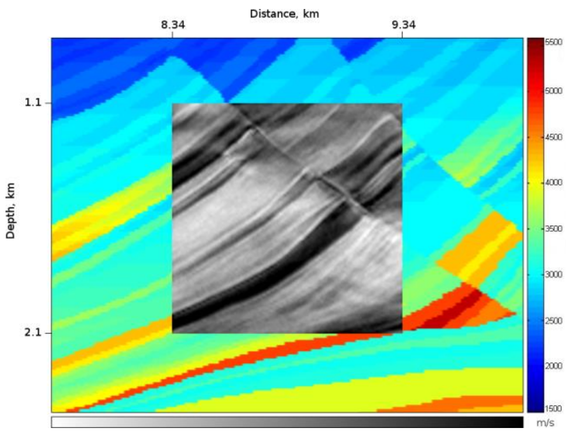

Figure 7: VPRTM. IVPIC (3f) for the part of the Marmousi2 model.

Field Data Example

The result of the conventional RTM for one of the oilfields in the West Siberia is presented on Fig. 8. Strong reflections in the middle of the section correspond to the Bazhenov formation with the tight oil (green line). The minimal variances are presented on Fig. 9, IVPIC (3e). This IVPIC (3e) is a measure of irregularity of scattered waves in each point per se. The strongest scattering zones (see Fig. 9) are located at the basement top (red line). Oil well drilling to these zones (black vertical line) gave oil debits almost one order more than the Bazhenov formation.

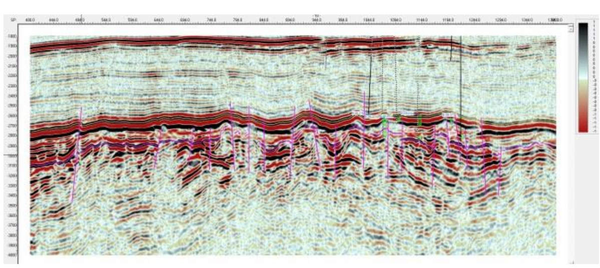

Figure 8: Conventional RTM

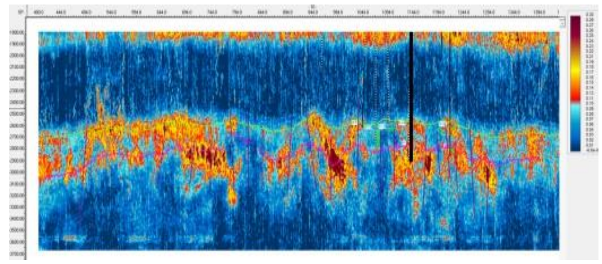

Figure 9: VPRTM. Minimal variances IVPIC (3e).

Conclusion and Discussion

The solutions of the forward and adjoint problems are based on the first-order equations. This allows one operate at each point of space in the area of the first arrivals with pairs of interconnected vectors depending on time and sources. Filtering the interconnected vector pairs in the amplitude and phase domain determines the admissible set of pairs. Application of this set of interconnected vector pairs image conditions allows us to generate subsurface images which are more informative than conventional RTM images. The VPRTM method with phase filtering demonstrates high sensitivity to velocity variations. Method is perspective for carrying out amplitude versus angle analysis, migration velocity analysis and may be basis for a new scattering versus angle analysis.

Acknowledgments

The authors thank V.Filatova and V.Sedaikina for useful participation. This work is supported by the Russian Science Foundation under grant 16-11-10027.

EDITED REFERENCES

Note: This reference list is a copyedited version of the reference list submitted by the author. Reference lists for the 2017 SEG Technical Program Expanded Abstracts have been copyedited so that references provided with the online metadata for each paper will achieve a high degree of linking to cited sources that appear on the Web.

REFERENCES

Alkhalifah, T., 2015, Scattering-angle based filtering of the waveform inversion gradients: Geophysical Journal International, 200, 363–373, http://doi.org/10.1093/gji/ggu379.

Alekseev, A. S., and G. N. Erokhin, 1989, Integation in geophysical inverse problems (Integrated Geophysics): USSR Academy of Sciences Proceedings, **308**, UDC 550.3:517.97, 1327–1331.

Anikonov, Yu. E., B. A. Bubnov, and G. N. Erokhin, 1997, Inverse and ill-posed sources problems: VSP.

Baysal, E., D. D. Kosloff, and J. W. C. Sherwood, 1983, Reverse time migration: Geophysics, **48**, 1514–1524, http://doi.org/10.1190/1.1441434.

Erokhin, G. N., A. N. Kremlev, L. E Starikov, V. V. Maltcev, and S. E. Zdolnik, 2012, CSP-method prospecting of fracture-cavernous reservoirs in the Bazhen formation of the Salym oilfield: 74th Annual International Conference and Exhibition, EAGE, Extended Abstracts, Y028.

Kremlev, A. N., G. N., Erokhin, L. E. Starikov, and S. V. Rodin, 2011, Fracture and cavernous reservoirs prospecting by the CSP prestack migration method: 73rd Annual International Conference and Exhibition, EAGE, Extended Abstracts, B024, https://doi.org/10.3997/2214-4609.20148996.

Khaidukov, V., E. Landa and T. J. Moser, 2004, Diffraction imaging by focusing-defocusing: an outlook on seismic super resolution: Geophysics, **69**, 1478–1490, https://doi.org/10.1190/1.1836821.

Landa, E., V. Shtivelman, and B. Gelchinsky, 1987, A method for detection of diffracted waves on common-offset sections: Geophysical Prospecting, **35**, 359–374, http://doi.org/10.1111/j.1365-2478.1987.tb00823.x.

McMechan, G. A., 1983, Migration by extrapolation of time-dependent boundary values: Geophysical Prospecting, **31**, 413–420, http://doi.org/10.1111/j.1365-2478.1983.tb01060.x.

Pierce, A. D., 1989, Acoustics: An Introduction to Its Physical Principles and Applications: Acoustical Society of America.

Plessix, R.-E., 2006, A review of the adjoint-state method for computing the gradient of a functional with geophysical applications: Geophysical Journal International, **167**, 495–503, http://doi.org/10.1111/j.1365-246X.2006.02978.x.

Sava, P., and S. Fomel, 2006, Time-shift imaging condition in seismic migration: Geophysics, **71**, no. 6, S209–S217, https://doi.org/10.1190/1.2338824.

Stolk, C. C., M. V. de Hoop, and T. Op't Root, 2009, Linearized inverse scattering based on seismic reverse-time migration: Proceedings of the Project Review, Geo-Mathematical Imaging Group: Purdue University, 91–108.

Symes, W. W., 2007, Reverse time migration with optimal checkpointing:Geophysics, **72**, no. 5, SM213–SM221, http://doi.org/10.1190/1.2742686.

Vyas, M., D. Nichols, and E. Mobley, 2011, Efficient RTM angle gathers using source directions: 81st Annual International Meeting, SEG, Expanded Abstracts, 3104–3108, https://doi.org/10.1190/1.3627840.

Whitmore, N. D., 1983, Iterative depth migration by backward time propagation: 53rd Annual International Meeting, SEG, Extended Abstracts, 382–385.

Whitmore, N. D., and S. Crawley, 2012, Applications of RTM inverse scattering imaging conditions: 82nd Annual International Meeting, SEG, Expanded Abstracts, http://doi.org/10.1190/segam2012-0779.1.

Xie, X., and R. S. Wu, 2002, Extracting angle domain information from migrated wavefields: 72nd Annual International Meeting, SEG, Expanded Abstracts, 1360–1363, https://doi.org/10.1190/1.1816910.
Xie, X. B., 2015, An angle-domain wavenumber filter for multi-scale full-waveform inversion: 85th Annual International Meeting, SEG, Expanded Abstracts, 1132–1137, http://doi.org/10.1190/segam2015-5877023.1.
Yan, R., H. Guan, X.-B. Xie, and R.-S. Wu, 2014, Acquisition aperture correction in the angle domain toward true-reflection reverse time migration: Geophysics, **79**, no. 6, S241–S250, http://doi.org/10.1190/geo2013-0324.1.
Yan, R., and X.-B. Xie, 2009, A new angle-domain condition for prestack reverse-time migration: 79nd Annual International Meeting, SEG, Expanded Abstracts, 2784–2788, https://doi.org/10.1190/1.3255427.
Yoon, K., and K. J. Marfurt, 2006, Reverse-time migration using the Poynting vector: Exploration Geophysics, **37**, 102–107.
Zhang, Q., and G. A. McMechan, 2011, Direct vector-field method to obtain angle-domain common-image gathers from isotropic acoustic and elastic reverse time migration: Geophysics, **76**, no. 5, WB135–WB149, http://doi.org/10. 1190/geo2010-0314.1.
Zhu, X., and R. Wu, 2008, Imaging diffraction points using the local image matrix in prestack migration: 78th Annual International Meeting, SEG, Expanded Abstracts, 2161–2165, https://doi.org/10.1190/1.3063853.